Erratum

A thermodynamic approach to alamethicin pore formation

Asif Rahaman, Themis Lazaridis *

Department of Chemistry, City College of New York, 160 Convent Avenue, New York, NY 10031, USA

ARTICLE INFO

ABSTRACT

The structure and energetics of alamethicin Rf30 monomer to nonamer in cylindrical pores of 5 to 11 Å radius are investigated using molecular dynamics simulations in an implicit membrane model that includes the free energy cost of acyl chain hydrophobic area exposure. Stable, low energy pores are obtained for certain combinations of radius and oligomeric number. The trimer and the tetramer formed 6 Å pores that appear closed while the larger oligomers formed open pores at their optimal radius. The hexamer in an 8 Å pore and the octamer in an 11 Å pore give the lowest effective energy per monomer. However, all oligomers beyond the pentamer have comparable energies, consistent with the observation of multiple conductance levels. The results are consistent with the widely accepted "barrel-stave" model. The N terminal portion of the molecule exhibits smaller tilt with respect to the membrane normal than the C terminal portion, resulting in a pore shape that is a hybrid between a funnel and an hourglass. Transmembrane voltage has little effect on the structure of the oligomers but enhances or decreases their stability depending on its orientation. Antiparallel bundles are lower in energy than the commonly accepted parallel ones and could be present under certain experimental conditions. Dry aggregates (without an aqueous pore) have lower average effective energy than the corresponding aggregates in a pore, suggesting that alamethicin pores may be excited states that are stabilized in part by voltage and in part by the ion flow itself.

1. Introduction

Alamethicin (ALM) is a 20-residue antimicrobial peptide produced by the soil fungus *Trichoderma viride* that is rich in α-amino isobutyric acid (Aib) and forms voltage-gated ion channels [1,2]. The crystal structure of ALM showed an α-helix from the N-terminus to Pro 14 and a 3_{10} helix from Pro 14 to the C-terminus [3]. The fact that ALM-induced ion conductivity appears at discrete levels [4] has been attributed to formation of transient "barrel-stave" pores consisting of a variable number of monomers around a central aqueous pore [5,6]. Various propositions have been made for the voltage dependent step: partition into the bilayer, transition from an interfacial to a transmembrane (TM) orientation, conformational change, further immersion into the bilayer, flipping of helices from an antiparallel to a parallel orientation, or aggregation [2,7,8].

A variety of experimental techniques have been employed to understand the mechanism of ion channel formation by ALM. Its ion conductance properties have been investigated under different conditions [9–11], including covalent tethering [12]. Some studies with model membranes suggested an interfacial orientation [13–15], while others found a TM orientation [16,17], a highly tilted orientation [18], or a distribution of orientations [19]. Other studies

detected both orientations depending on peptide concentration and hydration [20–22]. Conflicting findings have also been reported on the aggregation state of ALM in membranes in the absence of voltage, with some studies finding predominantly monomers [23–25], while others detected oligomers [26–30], with aggregation diminishing at higher temperatures [31]. Low-resolution information on the structure of the ALM pore has been obtained by neutron scattering. It was found that in DLPC the pores are made of 8–9 helical peptides arranged in parallel around an 18 Å diameter water-filled pore [32]. Somewhat larger pores were obtained in DPhPC. Indirect information on the pore size has also been obtained by studying the effect of polymers on the observed conductance [33]. The barrel stave model is widely accepted, but not universally [10,14].

ALM has also been the subject of numerous theoretical studies. Models of the channel have been constructed with restrained molecular dynamics (MD) in an implicit bilayer [34] or in vacuum with a few explicit water molecules [35]. Explicit solvent MD simulations have also been performed on monomers in water and/or methanol [36,37] and inserted [37,38] or adsorbed [39,40] on lipid bilayers or octane slabs. Simulations of ALM oligomers in lipid bilayers have also been performed [41–43]. The authors suggested that the tetramer does not conduct ions and that the lowest conductance level likely corresponds to a pentamer. Most stable in the simulations was found to be the hexamer. A more recent coarse-grained and atomistic MD study found extensive aggregation of ALM in a lipid bilayer [44]. The peptides exhibited occasional transitions between the membrane spanning and the surface

bound configurations. Continuum electrostatics analysis showed the TM orientation to be more stable than the interfacial orientation [45] and that many channel structures obtained by MD are thermodynamically unstable in the membrane [46].

In previous work from our group, MD simulations in implicit membrane produced two possible orientations of similar energies: a tilted orientation at the interface with the N terminus partially inserted and a more fully inserted, TM orientation with the N terminus almost crossing the membrane [47]. The transfer energy from water to the membrane was large enough to ensure that all ALM partitioned to the membrane at reasonable concentrations. These results were in agreement with a variety of experimental studies suggesting that ALM penetrated the hydrophobic core of the bilayer even in the absence of voltage [1]. Also, that the TM orientation did not completely cross the membrane was in agreement with a spin-labeling EPR study [48]. Voltage did not produce significant change in these structures but shifted the equilibrium towards the TM orientation by 0.8–0.9 kcal/mol [47]. More recently we found that inclusion of the membrane dipole potential [49] or lateral pressure effects [50] makes the interfacial configuration more parallel to the membrane.

Although ALM has been studied extensively, the pore structure in the membrane is still under debate. All atom MD studies have probed the kinetic stability of model pore structures, but have not yet provided information on their thermodynamic stability due to the large computational expense. Here, we attempt to do just that by introducing new methodology based on implicit membrane modeling. We construct models of different oligomeric numbers around pores of different sizes and compute the average effective energy per monomer. The implicit model also allows us to easily assess the effect of external voltage and evaluate proposed mechanisms of voltage dependence. Further, comparison with the energies of dry aggregates allows us to investigate the nature of the closed state and the energetics of the opening transition.

2. Methods

2.1. Implicit membrane model

We performed MD simulations with IMM1, an effective energy function for proteins in lipid membranes [51], which is an extension of EEF1 for water-soluble proteins [52]. Effective energy (W) is the free energy of a given, fixed protein conformation and is obtained as the sum of the intramolecular energy (E) and the solvation free energy (ΔG^{slv}). EEF1 uses the extended atom CHARMM force field (param19) [53] with neutralized ionic side chains and a linear distance dependent dielectric constant ($\varepsilon = r$) for the electrostatic interactions. IMM1 extends EEF1 to heterogeneous membrane–water systems by allowing the solvation parameters to vary between values corresponding to aqueous solution and values corresponding to cyclohexane. The membrane is considered to be parallel to the xy plane with its center at $z = 0$. The solvation parameters of all atoms (ΔG_i^{ref}) depend on the vertical position, $z' = |z| / (T / 2)$, where T is the thickness of the nonpolar core of the membrane. To account for the strengthening of electrostatic interactions in the membrane, a modified dielectric screening function is used

$$\varepsilon = r^{f_{ij}} \quad f_{ij} = a + (1-a)\sqrt{f_i f_j} \tag{1}$$

where f_i and f_j are given as

$$f(z') = \frac{z'^n}{1 + z'^n}. \tag{2}$$

The switching function f describes the transition from one phase to the other and n controls the steepness of the transition. The exponent

$n = 10$ gives a region of 6 Å over which the environment transitions from 90% nonpolar to 90% polar. The value 0.85 for the adjustable parameter a was found to give membrane binding energies in accord with experiment. Modeling of proteins with an aqueous pore was made possible by making the switching function dependent on the distance from the z axis [54,55]:

$$F(z', r') = f(z') + h(r') - f(z') + h(r') \quad , h(r) = 1 - \frac{r'^n}{1 + r'^n}, \quad r'$$
$$= r/R, \quad r = \sqrt{x^2 + y^2} \tag{3}$$

where r is the distance of any atom from the center of the pore and R the radius of the pore. The resulting energy function was referred to as IMM1-pore and was shown to discriminate the correct fold of TM beta barrels [54].

2.2. Extension to the all-atom CHARMM 36 force field

The EEF1 and IMM1 functions are based on the "united atom" CHARMM 19 force field in which the nonpolar hydrogen atoms are not explicitly represented. While this approximation is reasonable, it may affect the packing energies [56]. Indeed, interactions between TM helices sometimes appear too strong with this energy function. In addition, it does not allow one to take advantage of the progress in parameterization that took place over the last 15 years. For these reasons, IMM1 was adapted to the most recent, all-atom force field, referred to as CHARMM 36 [57]. This was done by transferring the solvation parameters from the atom types of CHARMM 19 to the corresponding atom types in CHARMM 36 and modifying the partial charges of the ionizable residues in CHARMM 36 to match those in IMM1.

One more change was necessary. CHARMM 19 scales the 1–4 interactions (the interactions between atoms separated by three bonds) by 0.4, while the all-atom CHARMM force fields do not scale them at all. This affects significantly the transfer energies from water to the membrane because IMM1 uses a position-dependent dielectric constant for all electrostatic interactions (Eq. (1)). Without the scaling of 1–4 interactions, IMM1 gives very little electrostatic stabilization in the membrane. Thus, the code was modified so that 1–4 interactions are excluded from the scaling in Eq. (1) and the value of the parameter a was adjusted to 0.91 to obtain roughly the same electrostatic stabilization in the membrane as with the original IMM1. This version is referred to as IMM1-p36.

2.3. Free energy of hydrophobic exposure

In its standard form, IMM1-pore produced distorted ALM oligomeric structures in cylindrical pores with monomers highly tilted. We hypothesized that this is due to the neglect of the free energy cost of hydrophobic exposure of lipids when the pore is not completely lined with peptide. To include this free energy cost, the effective energy (W) was modified as follows:

$$W = E + \Delta G^{slv} + E^{pore} \tag{4}$$

where E^{pore} is the residual pore energy and it is expressed as

$$\frac{E^{pore}}{\gamma} = 2\pi RT - \sum_i \left(1 - f(z_i')\right) \exp\left(-\frac{(r_i - R)^2}{\beta}\right) \pi r_i^{vdw^2} \tag{5}$$

where γ is the hydrocarbon–water interfacial tension, for which we chose the value 50.05 mN/m [58], and R is the radius of the pore. The first term on the right-hand side, multiplied by γ, corresponds to the classical pore formation energy for a membrane with thickness T. This is the energy of the "naked" pore (no peptides present). The second term in Eq. (5) represents the lowering of the free energy due to

coverage of hydrophobic area by peptides. $1.66\sqrt{\beta}$ is the width of the Gaussian distribution, set at 0.7, such that when peptides align completely around the pore E^{pore} vanishes. r_i is the distance of any atom i from the center of the pore (z axis), and r_i^{vdw} is the van der Waals radius of atom i. E^{pore} should be positive and should approach zero when the peptides cover up the pore completely.

2.4. Computational protocols

New Aib and terminal phenylalaninol residues were created in the CHARMM 36 force field. The structure of ALM Rf30 (with Glu at position 18) was obtained from the PDB (ID: 1AMT). This crystal structure has some 3_{10} helical character near the C terminus, which in our simulations converts rapidly to α-helical. First, a single monomer of ALM was equilibrated in pores ranging from 5 to 11 Å radius. Then, different oligomeric states of ALM in the pore were created by rotating the equilibrated monomers N times by an angle 360°/N. The energies of these assemblies were then energy-minimized. For smaller pore radii, when a large number of peptides were placed, a large van der Waals stress was created. To relieve this stress, the peptides were placed in a larger radius pore initially and then equilibrated. To obtain "dry" aggregates (oligomers without a pore), the initial structures of the corresponding oligomers in the pore were placed in the membrane (without a pore) and then subjected to MD. The width of the lipid membrane was 26 Å in all simulations. Each system was simulated for 3 ns, 1 ns of which was used for equilibration and the following 2 ns for data collection and averaging (plots of the energy vs time show that the energy converges after 1 ns and a 10-ns simulation of a hexamer produced results within the statistical uncertainty). Statistical errors were calculated as the standard deviation of averages calculated over four 0.5-ns periods. The temperature was maintained at 298.15 K using the Nosé–Hoover thermostat. The SHAKE algorithm was used to constrain high frequency bonds with hydrogen atoms, allowing a time-step of 2 fs for the Verlet integration.

3. Results

3.1. Oligomers in the absence of an aqueous pore

The structures of a few representative dry oligomers are shown in Figs. 1 (heptamer) and S1 (tetramer, nonamer). They all form close-packed bundles. With increasing aggregate size, some ALM molecules adopt interfacial orientations. It is interesting that, whereas monomers and low oligomers do not cross the membrane completely, pentamer and higher oligomers do. The average effective energy and its components for "dry" oligomers are given in Table S1 and plotted in Fig. 2. The total effective energy decreases monotonically from monomer to pentamer. Beyond the pentamer the variation in energy is small and
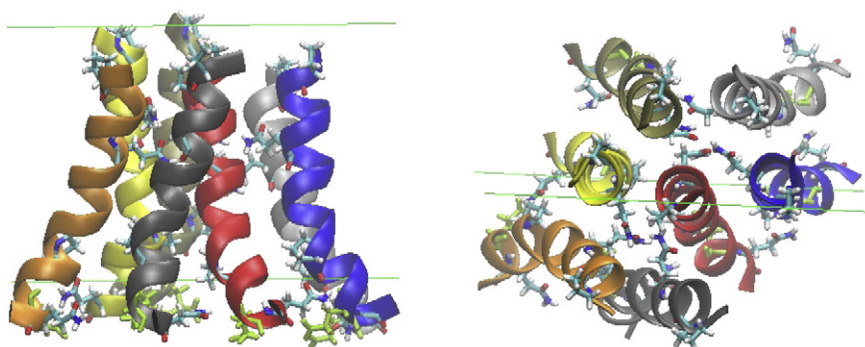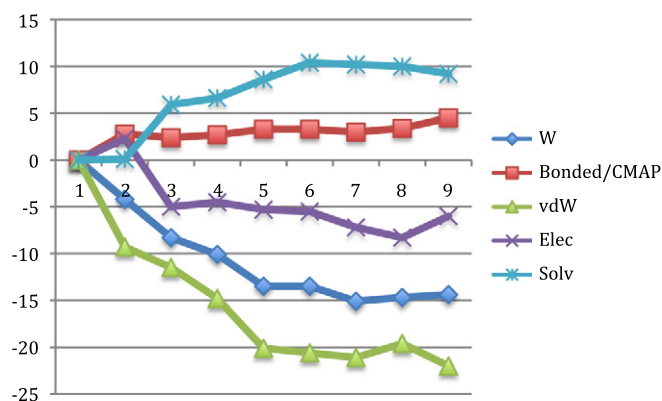

Fig. 2. Total effective energy (W) and its components (bonded, van der Waals, electrostatic, and solvation) per monomer as a function of oligomeric number in dry aggregates. All values are in kcal/mol and relative to the monomer.

beyond the heptamer within statistical error. The drop in energy from monomer to pentamer is substantial, about 14 kcal/mol per monomer, mostly due to van der Waals energy and, to a smaller extent, electrostatic energy. The solvation energy term opposes association, as expected. The bonded energy is slightly higher for the oligomers than the monomer, as each monomer strains to optimize intermolecular interactions.

3.2. Oligomers in the presence of an aqueous pore

The energies of ALM oligomers in cylindrical pores of different radii are given in Table 1. For monomer and dimer the average energy increases monotonically with increasing pore radius, primarily due to E^{pore} (a larger amount of pore surface remains exposed as the radius increases). The higher oligomers show at least one minimum in energy per monomer as the radius increases. The trimer and the tetramer show a minimum at pore radius 6 Å. The pentamer shows two minima. The first is at radius 5 Å but the structure of the oligomer is distorted and the pore is closed. The second minimum at radius 7 Å corresponds to a regular barrel-stave structure with an open pore. Similarly for the heptamer and the octamer, the lowest minimum corresponds to a small pore with additional monomers on the periphery and the second lowest minimum corresponds to a single layer of peptide lining a larger pore. Such structures are indicated by an underline in Table 1. Note that the energies of the dry oligomers, also shown in Table 1, are in most cases slightly lower than the energies of the best pore structures (see Discussion).

The components of the energy for the optimal oligomers are shown in Table S2 and plotted in Fig. 3. As with the dry oligomers (Fig. 2), the van der Waals and electrostatic energies decrease substantially as the

Fig. 1. Average structure of the dry heptamer. Side and top views are shown. The green lines represent the boundaries of the hydrophobic membrane interior. Gln, Glu and Pro residues are represented as sticks, Glu in green and Gln and Pro in multicolor bonds.

Table 1
Average effective energy per monomer (kcal/mol) for alamethicin oligomers in cylindrical pores of radius R (in Å) and in the absence of a pore (dry aggregates).

Number of alamethicin molecules	$R = 5$	$R = 6$	$R = 7$	$R = 8$	$R = 9$	$R = 10$	$R = 11$	$R = 12$	Dry aggregates
1	212.7 ($\pm$1.0)	223.8 ($\pm$0.5)	236.7 ($\pm$1.1)	252.2 ($\pm$1.6)	260.5 ($\pm$1.1)	276.4 ($\pm$/1.6)	287.6 ($\pm$0.8)	301.7 ($\pm$1.1)	176.9 ($\pm$0.6)
2	180.0 ($\pm$1.4)	187.1 ($\pm$1.9)	191.7 ($\pm$0.3)	201.4 ($\pm$1.1)	204.8 ($\pm$0.6)	213.3 ($\pm$0.4)	216.9 ($\pm$2.4)	222.4 ($\pm$1.4)	172.7 ($\pm$1.5)
3	175.8 ($\pm$0.2)	173.0 ($\pm$0.9)	180.5 ($\pm$1.9)	180.2 ($\pm$0.9)	186.2 ($\pm$0.5)	191.2 ($\pm$0.8)	196.2 ($\pm$0.8)	198.8 ($\pm$1.5)	168.6 ($\pm$1.0)
4	170.8 ($\pm$1.5)	169.3 ($\pm$0.7)	169.8 ($\pm$0.9)	173.4 ($\pm$2.2)	176.4 ($\pm$0.3)	179.5 ($\pm$1.2)	183.3 ($\pm$0.9)	186.8 ($\pm$0.7)	166.8 ($\pm$0.5)
5	163.7 ($\pm$1.6)	167.2 ($\pm$1.0)	165.4 ($\pm$1.0)	165.9 ($\pm$0.8)	170.4 ($\pm$0.6)	173.7 ($\pm$0.9)	177.3 ($\pm$0.3)	177.9 ($\pm$0.3)	163.3 ($\pm$0.5)
6	165.2 ($\pm$1.2)	163.5 ($\pm$0.6)	163.6 ($\pm$0.5)	163.5 ($\pm$0.6)	165.2 ($\pm$0.3)	170.5 ($\pm$0.1)	170.3 ($\pm$0.7)	173.0 ($\pm$0.8)	163.4 ($\pm$0.6)
7	165.1 ($\pm$0.9)	164.6 ($\pm$0.4)	165.4 ($\pm$0.6)	166.3 ($\pm$0.4)	165.2 ($\pm$0.5)	165.3 ($\pm$0.5)	166.0 ($\pm$0.7)	168.4 ($\pm$0.3)	161.8 ($\pm$0.8)
8	162.0 ($\pm$0.5)	160.9 ($\pm$0.4)	164.0 ($\pm$0.4)	166.4 ($\pm$0.3)	163.6 ($\pm$1.5)	165.4 ($\pm$0.5)	163.3 ($\pm$0.6)	166.5 ($\pm$0.2)	162.2 ($\pm$0.9)
9	178.6 ($\pm$0.7)	166.5 ($\pm$0.2)	164.9 ($\pm$0.4)	166.6 ($\pm$1.8)	165.3 ($\pm$0.6)	164.7 ($\pm$0.4)	164.6 ($\pm$0.5)	164.6 ($\pm$0.4)	162.5 ($\pm$0.6)

The underline indicates lowest energy structures or, for larger aggregates, lowest energy open pore structures. They are referred to as "optimal" in the remainder of the article.

oligomeric number increases. Here, the solvation component includes the pore energy due to acyl chain exposure, and that is why this component drops significantly from monomer to dimer. The contribution of the added term, E^{pore} to the total energy for pore radius $R = 9$ Å and varying number of oligomers is given in Table S3. The "naked pore" energy (when there is no peptide in the pore) at this radius is 105.9 Å ($2\pi RT\gamma$, $T = 26$ Å). Addition of peptides covers hydrophobic lipid area and reduces the pore energy. The residual pore energy per monomer decreases with the increase in number of monomers and reaches a plateau after the pore is filled with peptides. The parameters of this term were chosen so that the pore energy for a completely lined pore will be close to zero, but there is no simple way to make it exactly zero. The fact that the pore energy becomes slightly negative at larger oligomeric numbers is an artifact of the approach taken to account for hydrophobic area exposure.

Fig. S2 shows the average structures of monomer and dimer in a pore of radius 5 Å. Both monomer and dimer aligned to the side of the cylindrical pore with hydrophobic residues facing the membrane and the hydrophilic residues like Gln and Glu facing water. In the monomer, both Gln residues face the center of the pore. In the dimer, one of the Gln and Glu residues near the C terminus moves towards bulk water. Fig. S3 shows the average structures of the trimer and tetramer, which at their optimal radius seem to form closed pores.

Fig. 4 shows the average structure of a heptamer corresponding to the most stable open pore. Structures of pentamer to nonamer are given in Fig. S4. In these structures the Gln 7 residues point towards the lumen of the pore whereas the Gln and Glu residues near the C-terminus point towards bulk water. For all these oligomers, it was proposed that the Gln residues form an annular ring in the pore that stabilizes the pore structure [3]. Our simulations do not show such regular h-bonded rings. One of the Gln residues often h-bonds to the backbone nitrogen atom of another monomer. A representative broken h-bond network is shown in Fig. 4. Other times the Gln residues prefer to h-

bond vertically, causing a vertical shift of one monomer relative to the other (e.g. Fig. S4e). As a result, the centers of mass of the helices are not always on the same membrane depth.

To determine the shape of the oligomeric bundles in a quantitative way we calculated average tilt and kink angles for the two portions of the molecule on either side of Pro 14, which is on average about 4 Å below the hydrocarbon–polar interface. The Nt tilt angle is defined as the angle between the membrane normal (positive z semiaxis) and the helix axis defined by the residues from Pro 14 to the N-terminus. The Ct tilt angle is defined as the angle between the negative z semiaxis and the helix axis defined by the residues from Pro 14 to the C-terminus. The kink angle is the angle between the axes of the two portions of the molecule. The results are shown in Table 2. The kink angle tends to be smaller than in the crystal structure (153.7, 158.2, 163.4 for the three molecules in the asymmetric unit). That is, the molecule is on average more kinked than in the crystal structure. The Nt tilt angle is significantly smaller than the Ct tilt angle. If the former was zero and the latter positive, then the shape of the bundle would be funnel-like, with the Nt helix lining the pore and the Ct helix forming the mouth of the funnel. Equal values of the Nt and Ct angles would make the shape of the pore hourglass-like. The actual situation is between the two ideals, so we may characterize the shape of these bundles as a hybrid between hourglass and funnel.

3.3. Effect of transition region width

The value of n in Eqs. (2) and (3) determines the width of the transition region between hydrocarbon and water. The value 10 gives a transition region of ~6 Å going from 90% polar to 90% nonpolar for a typical membrane with 26 Å thickness. One disadvantage of the mathematical model we use is that the width of the transition region changes with the thickness of the membrane or the radius of the pore. Thus, when we compare pores with large differences in R the transition width could change substantially and that could affect the resulting energies (in general, a steeper transition gives more favorable energies for amphipathic peptides). The same value of $n = 10$ for a cylindrical pore with a radius of 5 Å gives a transition region of 2.2 Å going from 90% polar to 90% nonpolar. To examine the effect of transition region thickness in the absence of statistical noise, we performed single-point energy calculations on the final structure of the trajectory for each oligomer with n adjusted to obtain a transition region of ~6 Å. The results are shown in Table S4. Indeed, the reduction in transition region thickness lowers the energy. The difference is almost 4 kcal/mol for the monomer and diminishes gradually in larger pores.

In principle, the transition region thickness for a cylindrical, hydrophobic pore need not be the same as that for the membrane interface. In the former there is a transition from the acyl chains to water, whereas in the latter there is a transition from the acyl chains to the polar head groups. It is reasonable to expect that the former might be somewhat sharper than the latter. However, whatever the transition region thickness is in the pore, it clearly should not be dependent on the radius. Therefore, in the remainder of this work we use n values adjusted to
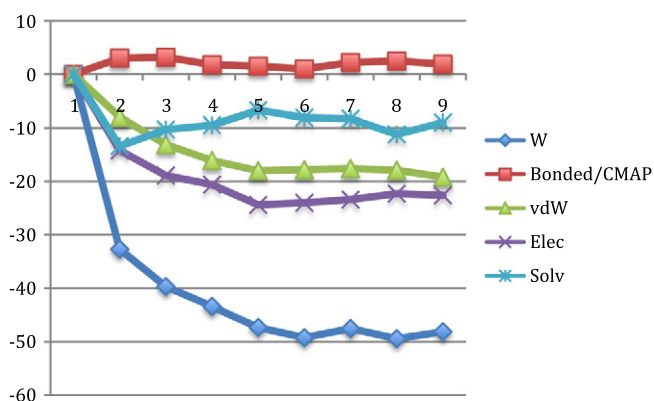

Fig. 3. Total effective energy (W) and its components (bonded, van der Waals, electrostatic, and solvation) per monomer as a function of oligomeric number in optimal pore structures. All values are in kcal/mol and relative to the monomer.
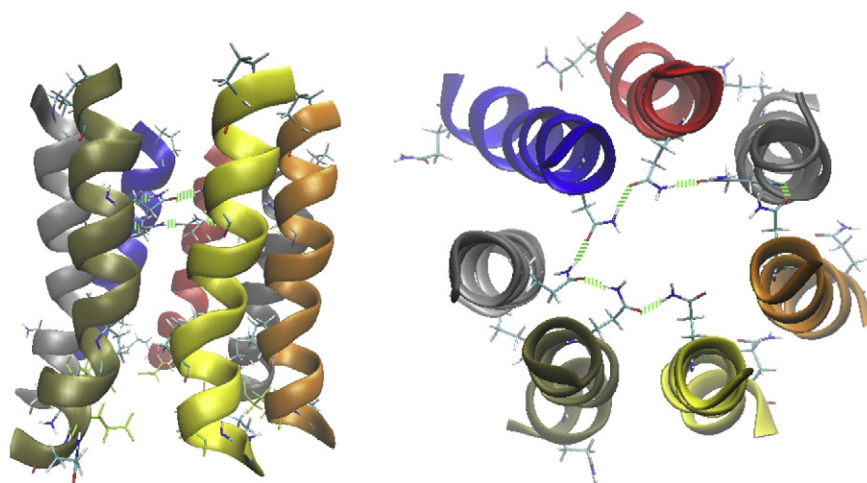
Fig. 4. Side and top views of a heptamer in a pore of 9 Å showing the broken hydrogen bond network involving Gln 7. One of the monomers forms a hydrogen bond with the backbone of the others disrupting the annular ring. Green broken lines are the hydrogen bonds.

maintain the same transition region thickness to avoid any bias in favor of smaller pores.

3.4. Translational and rotational entropy contributions

As almost all side chains in ALM are short, we neglect the conformational entropy loss upon oligomerization. The entropy loss due to translational and rotational motions of aggregates was determined from the probability distributions of the center of mass positions and peptide orientations, respectively, as in previous work [59]. The results are tabulated in Table S5. Their values range from 3.5 to 7 kcal/mol and increase gradually as the oligomeric number increases. These values are probably overestimates because the reference state for the calculations is free rotation and translation at 1 M concentration and neglect the constraints of the membrane. Addition of this contribution favors the smaller aggregates but does not change substantially the picture obtained from the effective energy alone.

3.5. Effect of TM voltage

Simulations with a voltage of 0.1 V, positive on the side of the C-terminus, were performed for the optimal ALM assemblies in Table 1. The average structures obtained were very similar to those in the absence of voltage. To investigate the effect of voltage on the energetics in the absence of statistical noise, we performed single-point energy calculations on the final structure from the trajectories. The results are shown in Table S6. There are two contributions to the difference in energy reported in this table. The first is from the Glu 18 residue and is about 0.1 V ∗ 1e ~ 2.3 kcal/mol. If the C terminus is in the +V direction the energy change is favorable, otherwise it is unfavorable. The second contribution is from helix dipole. In previous work we found that the dipole contribution stabilizes the TM configuration vs. the interfacial configuration by 0.8 to 0.9 kcal/mol when 0.1 V is applied. Similar results are obtained here. Application of voltage in a direction opposite to that of the helix dipole lowers the energy of the monomers in the

pore by 0.9 to 1 kcal/mol. The values in Table S6 are a combination of the above two contributions.

3.6. Antiparallel bundles

Because ALM makes ion channels only in the presence of *cis* positive voltage, which favors an orientation with the C terminus on the *cis* side, and because the C terminus is more hydrophilic and crosses the membrane with greater difficulty than the N terminus, it is usually assumed that ALM makes parallel helical bundles [1,5,42]. However, at higher concentrations in the absence of voltage and at later times when ALM molecules have translocated to the *trans* leaflet, antiparallel bundle formation seems possible. We thus constructed three antiparallel models: a dry tetramer, a dry hexamer, and a hexamer in a pore. The average energies of these models are shown in Table 3. It can be seen that in all cases considered the energy of the antiparallel model is lower than that of the corresponding parallel model, thanks to better van der Waals and electrostatic interactions. Fig. 5 shows the structure of the antiparallel hexamer in the pore and Fig. S5 shows the antiparallel dry tetramer.

4. Discussion

This work presents a new approach for analyzing barrel stave pore structures using implicit solvation modeling. This approach offers significant advantages compared to all-atom explicit simulations [42,60]. One advantage is the fast convergence. Within a few ns one can see whether a certain structure is stable or not. A second advantage is the ability to obtain estimates of the thermodynamic stabilities of the various structures. A third advantage is that it tests our understanding of the physical forces that play a role in peptide-induced pore formation. Of course, the approach is not without limitations. The implicit solvation model is highly approximate and the cylindrical shape of the pore is imposed at the outset. There is substantial experimental and theoretical evidence supporting this idea [60,61] but it is an assumption. The results

Table 2
Average tilt angles for the N-terminal (res. 1–14) and C-terminal (res. 14–20) helices (Nt tilt and Ct tilt, respectively) and kink angle between them for optimal oligomers in the pores.

	Monomer	Dimer	Trimer	Tetramer	Pentamer	Hexamer	Heptamer	Octamer	Nonamer
Nt tilt	9.4	14.0	14.9	12.3	13.2	22.8	16.1	26.8	15.0
Kink	150.6	145.1	131.7	134.7	131.2	124.9	138.7	123.8	134.5
Ct tilt	24.3	36.4	43.9	45.5	45.3	52.9	43.1	44.0	44.2

Table 3
Average total effective energy and its components (kcal/mol) for antiparallel and the corresponding parallel bundles (without voltage).

Energy components	Tetramer (dry−anti)	Tetramer (dry−para)	Hexamer (dry−anti)	Hexamer (in pore−anti)	Hexamer (dry−para)	Hexamer (in pore−para)
Total bonded energy/monomer	415.8 (±0.9)	416.2 (±0.1)	415.7 (±0.7)	416.1 (±0.4)	415.3 (±0.1)	415.9 (±0.4)
CMAP energy/monomer	−17.0 (±0.4)	−20.0 (±0.1)	−18.1 (±0.1)	−17.0 (±0.2)	−18.5 (±0.05)	−18.8 (±0.1)
van der Waals energy/monomer	−34.4 (±0.3)	−29.7 (±0.2)	−39.2 (±1.4)	−38.3 (±1.2)	−35.5 (±0.1)	−34.5 (±0.3)
Electrostatic energy/monomer	−134.9 (±3.5)	−126.3 (±0.1)	−133.7 (±1.8)	−121.0 (±1.1)	−127.3 (±0.1)	−112.5 (±1.6)
Solvation energy/monomer	−69.2 (±1.1)	−73.4 (±0.1)	−67.0 (±0.3)	−79.6 (±1.1)	−69.6 (±0.1)	−82.6 (±0.6)
Total effective energy/monomer	160.3 (±2.8)	166.8 (±0.5)	157.8 (±0.2)	160.2 (±1.4)	163.4 (±0.6)	167.4 (±1.5)

of studies like these should be treated as hypotheses to be tested by more detailed simulations and ultimately by experiment. Also, the membrane thickness has been treated as fixed, although it is known that it can locally adjust to improve the match between peptide and bilayer [62,63]. A rigorous correction for this, whereby one computes the energy in different membrane thicknesses and adds an estimate of the free energy of membrane deformation [45] could be pursued in the future for more accurate results.

There is a large body of experimental data that the present results can be compared with. Neutron scattering [32,64] and X-ray diffraction studies [61] suggested that ALM forms stable pores of about 8.5 Å inner radius and 19.4 Å outer radius consisting of 8 monomers. Our octamer has similar dimensions. However, our energy values for the oligomers above 5 are very similar, consistent with conductance studies that show multiple levels populated. Apparently, under certain experimental conditions, such as stacked bilayers and high peptide concentrations, one oligomeric state can dominate, for reasons that are not understood. A recent electrochemical STM study in monolayers was consistent with hexamers, with each ALM molecule shared between adjacent channels [65]. PELDOR studies of a backbone-labeled ALM analog detected a tetramer with 23 Å distance between the labels at position 16 [29,66]. Modeling such a tetramer, the authors obtained a distance of 18 Å. Our tetramer is even more compact, with distances between 11 and 16 Å. Distances of 23 Å in a tetramer would be possible in a pore of at least 10 Å radius, but that pore would have high energy because a lot of hydrophobic area would be exposed (Table 1).

Conductance measurements in membranes of different lipid composition showed that PE inhibits the formation of pores but increases the relative frequency of larger pores [11]. This finding could be theoretically explained assuming an hourglass shape of the ALM channel [67,68]. Previous modeling studies [69] reported aggregates that are more funnel-like. Our analysis suggests a hybrid between funnel and hourglass, which should be able to account for the lipid-dependence experiments. A more quantitative study could be performed using a recent model for lateral pressure effects [50].

Another source of experimental data with bearing on the pore structure is the pH dependence of conductance. Asami et al. [70] found that the presence of charge at residue 18 (Glu vs. Gln) does not have a major effect on conductance, whereas inserting a Glu at position 7 makes a dramatic difference. This is in agreement with the barrel stave model and the present structures. The effective pKa of Glu 18 in that study was around 4.5–5, indicating weak interactions between the Glu 18 residues and that at neutral pH all Glu 18 are ionized. This is in agreement with the work of Chiriac and Luchian [71]. In the present simulations Glu 18 was unprotonated. We note, of course, that in our implicit model the ionic residues do not carry a net charge, but only partial charges that reproduce the explicit solvent potential of mean force [51]. However, the average distance between the Glu 18 carboxyl groups in our oligomers is 9 Å or more, sufficient to weaken the repulsive interactions between them. Tieleman et al. found that they had to protonate some of the Glu 18 residues to obtain stable structures [42]. This may have been due to the proximity of these residues in the starting structures which created very strong repulsive forces. It would be interesting to repeat explicit simulations starting from structures obtained here.

It is often assumed that the alamethicin bundles are parallel [1,5,42]. The reason for this is the observation that channel opening occurs only at cis positive voltage and that this field would favor the translocation of the N terminus across the membrane. Conveniently, the N terminus is quite hydrophobic while the C terminus is very hydrophilic and thus would experience a high energy barrier in crossing the membrane. However, under conditions at which pore formation is not voltage dependent and after the initial formation of pores and the translocation of the ALM to the trans leaflet, this argument is no longer valid. Interestingly, we find antiparallel bundles to have lower effective energy than parallel ones. We should therefore consider the possibility that such bundles are formed under certain experimental conditions, such as dye leakage experiments in vesicles over a long period of time [72].

An extensively debated issue in ALM research is whether there exists a preaggregated, non-conducting state. Evidence in favor of aggregation
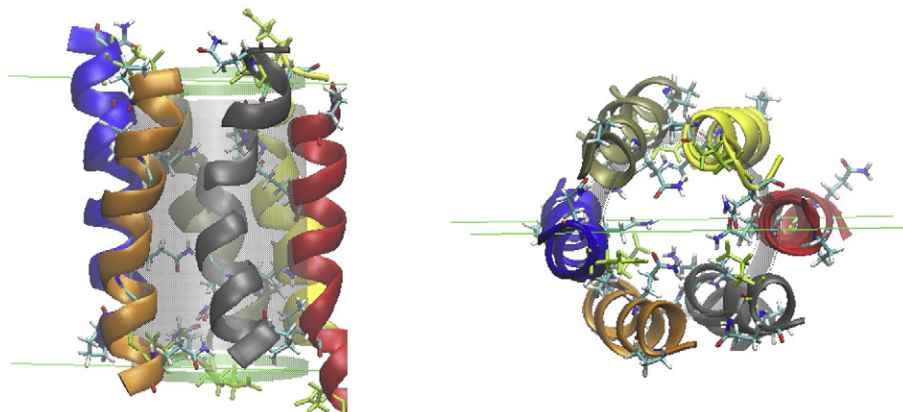

Fig. 5. Side and top views of the antiparallel hexamer in a pore of radius 8 Å. Graphic representations as in Fig. 1.

comes from the moderate dependence of relaxation kinetics on ALM concentration [73], the sigmoidal shape of binding isotherms [26,74], CD spectroscopy [27,31], 2-d aggregate formation on the surface of monolayers [14], solid state NMR at P/L = 1/100 [75] and at P/L 1:10 [76], PELDOR at P/L 1:160 to 1:50 [29], and X-ray scattering [30]. Rizzo et al. [74] estimated a critical P/L ~ 1:1000 for aggregation in the membrane. Leakage experiments showed sustained ability of ALM to form pores in the absence of voltage even down to P/L 1:2000 [72]. Evidence against aggregation in the absence of TM potential has been provided by EPR of spin-labeled ALM in vesicles at P/L from 1:600 to 1:7 [23,24] and at 1:100 in aligned bilayers [25] and studies with spin-labeled lipids at P/L 1:50 [77].

Our energies of association of ALM monomers are quite strong, with contributions from both van der Waals and electrostatic interactions. A strong interaction between ALM helices is plausible. Hydrogen bonding between polar residues in the membrane interior is known to provide a strong driving force for association [78,79]. In the case of ALM, the Gln 7 residues could provide a few kcal/mol of association energy. Nevertheless, it is possible that the association energies predicted by our implicit membrane model are overestimated. A more systematic study of association is needed, and the implicit simulation results need to be tested with explicit simulations. Previous application of IMM1 to other associating TM helices gave reasonable results [80,81]. It is noted, however, that a coarse-grained MD study also found extensive aggregation at P/L = 1:7 to 1:20 [44].

The present results indicate that the average effective energy of dry aggregates is lower than the corresponding oligomers in a pore, due mostly to electrostatic interactions. This result is not an artifact of the pore energy term, since this term is actually negative for large oligomers, i.e. it lowers the energy of the "wet" oligomers (Table S3). If that is true, the open states correspond to excited states. It should be noted here that the open pore states observed in conductance experiments are nonequilibrium states, whereas the closed states are equilibrium states. A widely accepted approach to compare the relative probability of an equilibrium and a nonequilibrium state is lacking. The concept of free energy is not well defined in nonequilibrium states, but there are attempts to do that. A generalization of the free energy that incorporates fluxes [82] shows that fluxes lower the generalized free energy of a nonequilibrium state. If this reasoning is correct, then one significant contribution to the stabilization of the open channel states is the nonequilibrium effect of ion flow. The fact that the ALM channel can conduct in the opposite direction when the voltage is rapidly reversed (becomes *cis* negative) [83] seems to support this idea. Reversal of the potential destabilizes the barrel but ion flow provides enough stabilization to keep it going for a while. Thus, it seems plausible that the ground state of ALM in membranes corresponds to closed aggregates and the open states are transiently stabilized by the "need" to dissipate electrochemical or chemical gradient. In this view, the "voltage-dependent step" is the ion or dye flow itself. We note, however, that open pores have also been observed under equilibrium conditions [32], which means that under certain conditions they can become ground states.

Thus, a lot remains to be clarified for a complete understanding of the ALM mechanism of membrane pore formation. First and foremost, the issue of aggregation in the closed state. It would be interesting to apply the TOXCAT technique [84] to measure directly the strength of association between two ALM monomers. On the theory side, we are planning to use potential of mean force calculations in explicit bilayers to test whether the implicit model predictions are correct, and if not, the origin of its failings. Another important but difficult goal for explicit simulation is the calculation of the free energy difference between dry and wet alamethicin bundles. The number of intriguing questions increases further when one considers other peptaibols. Some of them are much shorter than ALM, do they also form barrel stave aggregates? Why do some, like antiamoebin and trichotoxin, show only one conductance level [85] instead of the multiple levels of alamethicin?

Acknowledgements

References

[1] M.S. Sansom, The biophysics of peptide models of ion channels, Prog. Biophys. Mol. Biol. 55 (1991) 139–235.

[2] D.S. Cafiso, Alamethicin: a peptide model for voltage gating and protein–membrane interactions, Annu. Rev. Biophys. Biomol. Struct. 23 (1994) 141–165.

[3] R.O. Fox Jr., F.M. Richards, A voltage-gated ion channel model inferred from the crystal structure of alamethicin at 1.5-Å resolution, Nature 300 (1982) 325–330.

[4] L.G. Gordon, D.A. Haydon, The unit conductance channel of alamethicin, Biochim. Biophys. Acta 255 (1972) 1014–1018.

[5] G. Baumann, P. Mueller, A molecular model of membrane excitability, J. Supramol. Struct. 2 (1974) 538–557.

[6] G. Boheim, Statistical analysis of alamethicin channels in black lipid membranes, J. Membr. Biol. 19 (1974) 277–303.

[7] M.S. Sansom, Structure and function of channel forming peptaibols, Q. Rev. Biophys. 26 (1993) 365–421.

[8] H. Duclohier, H. Wroblewski, Voltage-dependent pore formation and antimicrobial activity by alamethicin and analogues, J. Membr. Biol. 184 (2001) 1–12.

[9] I. Vodyanoy, J.E. Hall, T.M. Balasubramanian, Alamethicin-induced current–voltage curve asymmetry in lipid bilayers, Biophys. J. 42 (1983) 71–82.

[10] J.E. Hall, I. Vodyanoy, T.M. Balasubramanian, G.R. Marshall, Alamethicin — a rich model for channel behavior, Biophys. J. 45 (1984) 233–247.

[11] S.L. Keller, S.M. Bezrukov, S.M. Gruner, M.W. Tate, I. Vodyanoy, V.A. Parsegian, Probability of alamethicin conductance states varies with nonlamellar tendency of bilayer phospholipids, Biophys. J. 65 (1993) 23–27.

[12] G.A. Woolley, Channel-forming activity of alamethicin: effects of covalent tethering, Chem. Biodivers. 4 (2007) 1323–1337.

[13] U. Banerjee, R. Zidovetzki, R.R. Birge, S.I. Chan, Interaction of alamethicin with lecithin bilayers: a 31P and 2H NMR study, Biochemistry 24 (1985) 7621–7627.

[14] R. Ionov, A. El-Abed, A. Angelova, M. Goldmann, P. Peretti, Asymmetrical ion-channel model inferred from two-dimensional crystallization of a peptide antibiotic, Biophys. J. 78 (2000) 3026–3035.

[15] V. Vitkova, P. Meleard, T. Pott, I. Bivas, Alamethicin influence on the membrane bending elasticity, Eur. Biophys. J. Biophys. 35 (2006) 281–286.

[16] C.L. North, M. Barranger-Mathys, D.S. Cafiso, Membrane orientation of the N-terminal segment of alamethicin determined by solid-state 15N NMR, Biophys. J. 69 (1995) 2392–2397.

[17] M. Bak, R.P. Bywater, M. Hohwy, J.K. Thomsen, K. Adelhorst, H.J. Jakobsen, O.W. Sørensen, N.C. Nielsen, Conformation of alamethicin in oriented phospholipid bilayers determined by 15N solid state nuclear magnetic resonance, Biophys. J. 81 (2001) 1684–1698.

[18] S.J. Ye, H.C. Li, F. Wei, J. Jasensky, A.P. Boughton, P. Yang, Z. Chen, Observing a model ion channel gating action in model cell membranes in real time in situ: membrane potential change induced alamethicin orientation change, J. Am. Chem. Soc. 134 (2012) 6237–6243.

[19] A. Spaar, C. Munster, T. Salditt, Conformation of peptides in lipid membranes studied by X-ray grazing incidence scattering, Biophys. J. 87 (2004) 396–407.

[20] H. Vogel, Comparison of the conformation and orientation of alamethicin and melittin in lipid membranes, Biochemistry 26 (1987) 4562–4572.

[21] H.W. Huang, Y. Wu, Lipid–alamethicin interactions influence alamethicin orientation, Biophys. J. 60 (1991) 1079–1087.

[22] K. He, S.J. Ludtke, W.T. Heller, H.W. Huang, Mechanism of alamethicin insertion into lipid bilayers, Biophys. J. 71 (1996) 2669–2679.

[23] S.J. Archer, J.F. Ellena, D.S. Cafiso, Dynamics and aggregation of the peptide ion channel alamethicin — measurements using spin-labeled peptides, Biophys. J. 60 (1991) 389–398.

[24] M. Barranger-Mathys, D.S. Cafiso, Collisions between helical peptides in membranes monitored using electron-paramagnetic-resonance — evidence that alamethicin is monomeric in the absence of a membrane-potential, Biophys. J. 67 (1994) 172–176.

[25] D. Marsh, M. Jost, C. Peggion, C. Toniolo, TOAC spin labels in the backbone of alamethicin: EPR studies in lipid membranes, Biophys. J. 92 (2007) 473–481.

[26] G. Schwarz, S. Stankowski, V. Rizzo, Thermodynamic analysis of incorporation and aggregation in a membrane: application to the pore-forming peptide alamethicin, Biochim. Biophys. Acta 861 (1986) 141–151.

[27] M. Cascio, B.A. Wallace, Conformation of alamethicin in phospholipid-vesicles — implications for insertion models, Proteins Struct. Funct. Genet. 4 (1988) 89–98.

[28] I. Vodyanoy, J.E. Hall, V. Vodyanoy, Alamethicin adsorption to a planar lipid bilayer, Biophys. J. 53 (1988) 649–657.

[29] A.D. Milov, R.I. Samoilova, Y.D. Tsvetkov, F. Formaggio, C. Toniolo, J. Raap, Self-aggregation of spin-labeled alamethicin in ePC vesicles studied by pulsed electron–electron double resonance, J. Am. Chem. Soc. 129 (2007) (9260–+).

[30] J.J. Pan, S. Tristram-Nagle, J.F. Nagle, Alamethicin aggregation in lipid membranes, J. Membr. Biol. 231 (2009) 11–27.

[31] G.A. Woolley, B.A. Wallace, Temperature dependence of the interaction of alamethicin helices in membranes, Biochemistry 32 (1993) 9819–9825.

[32] K. He, S.J. Ludtke, D.L. Worcester, H.W. Huang, Neutron scattering in the plane of membranes: structure of alamethicin pores, Biophys. J. 70 (1996) 2659–2666.

[33] S.M. Bezrukov, I. Vodyanoy, Probing alamethicin channels with water-soluble polymers — effect on conductance of channel states, Biophys. J. 64 (1993) 16–25.

[34] P.C. Biggin, J. Breed, H.S. Son, M.S. Sansom, Simulation studies of alamethicin–bilayer interactions, Biophys. J. 72 (1997) 627–636.

[35] J. Breed, P.C. Biggin, I.D. Kerr, O.S. Smart, M.S.P. Sansom, Alamethicin channels — modelling via restrained molecular dynamics simulations, Biochim. Biophys. Acta Biomembr. 1325 (1997) 235–249.

[36] N. Gibbs, R.B. Sessions, P.B. Williams, C.E. Dempsey, Helix bending in alamethicin: molecular dynamics simulations and amide hydrogen exchange in methanol, Biophys. J. 72 (1997) 2490–2495.

[37] D.P. Tieleman, M.S. Sansom, H.J. Berendsen, Alamethicin helices in a bilayer and in solution: molecular dynamics simulations, Biophys. J. 76 (1999) 40–49.

[38] D.P. Tieleman, I.H. Shrivastava, M.R. Ulmschneider, M.S.P. Sansom, Proline-induced hinges in transmembrane helices: possible roles in ion channel gating, Proteins Struct. Funct. Genet. 44 (2001) 63–72.

[39] D.P. Tieleman, H.J. Berendsen, M.S. Sansom, Surface binding of alamethicin stabilizes its helical structure: molecular dynamics simulations, Biophys. J. 76 (1999) 3186–3191.

[40] D.P. Tieleman, H.J.C. Berendsen, M.S.P. Sansom, Voltage-dependent insertion of Alamethicin at phospholipid/water and octane/water interfaces, Biophys. J. 80 (2001) 331–346.

[41] D.P. Tieleman, H.J. Berendsen, M.S. Sansom, An alamethicin channel in a lipid bilayer: molecular dynamics simulations, Biophys. J. 76 (1999) 1757–1769.

[42] D.P. Tieleman, B. Hess, M.S. Sansom, Analysis and evaluation of channel models: simulations of alamethicin, Biophys. J. 83 (2002) 2393–2407.

[43] D.P. Tieleman, V. Borisenko, M.S.P. Sansom, G.A. Woolley, Understanding pH-dependent selectivity of alamethicin K18 channels by computer simulation, Biophys. J. 84 (2003) 1464–1469.

[44] L. Thogersen, B. Schiott, T. Vosegaard, N.C. Nielsen, E. Tajkhorsid, Peptide aggregation and pore formation in lipid bilayer: a combined coarse-grained and all atom model, Biophys. J. 95 (2008) 4337–4347.

[45] A. Kessel, D.S. Cafiso, N. Ben-Tal, Continuum solvent model calculations of alamethicin–membrane interactions: thermodynamic aspects, Biophys. J. 78 (2000) 571–583.

[46] A. Kessel, D.P. Tieleman, N. Ben-Tal, Implicit solvent model estimates of the stability of model structures of the alamethicin channel, Eur. Biophys. J. Biophys. 33 (2004) 16–28.

[47] M. Mottamal, T. Lazaridis, Voltage-dependent energetics of alamethicin monomers in the membrane, Biophys. Chem. 122 (2006) 50–57.

[48] M. Barranger-Mathys, D.S. Cafiso, Membrane structure of voltage-gated channel forming peptides by site-directed spin-labeling, Biochemistry 35 (1996) 498–505.

[49] H. Zhan, T. Lazaridis, Influence of membrane dipole potential on peptide binding to lipid bilayers, Biophys. Chem. 161 (2012) 1–7.

[50] H. Zhan, T. Lazaridis, Inclusion of lateral pressure/curvature stress effects in implicit membrane models, Biophys. J. 104 (2013) 643–654.

[51] T. Lazaridis, Effective energy function for proteins in lipid membranes, Proteins Struct. Funct. Genet. 52 (2003) 176–192.

[52] T. Lazaridis, M. Karplus, Effective energy function for proteins in solution, Proteins 35 (1999) 133–152.

[53] E. Neria, S. Fischer, M. Karplus, Simulation of activation free energies in molecular systems, J. Chem. Phys. 105 (1996) 1902–1921.

[54] T. Lazaridis, Structural determinants of transmembrane beta-barrels, J. Chem. Theory Comput. 1 (2005) 716–722.

[55] M. Mihajlovic, T. Lazaridis, Antimicrobial peptides bind more strongly to membrane pores, Biochim. Biophys. Acta Biomembr. 1798 (2010) 1494–1502.

[56] J.M. Word, S.C. Lovell, J.S. Richardson, D.C. Richardson, Asparagine and glutamine: using hydrogen atom contacts in the choice of side-chain amide orientation, J. Mol. Biol. 285 (1999) 1735–1747.

[57] A.D. MacKerell Jr., M. Feig, I.C.L. Brooks, Extending the treatment of backbone energetics in protein force fields: limitations of gas-phase quantum mechanics in reproducing protein conformational distributions in molecular dynamics simulations, J. Comput. Chem. 25 (2004) 1400–1415.

[58] S. Zeppieri, J. Rodriguez, A.L.L. de Ramos, Interfacial tension of alkane plus water systems, J. Chem. Eng. Data 46 (2001) 1086–1088.

[59] J. Ramos, T. Lazaridis, Energetic determinants of oligomeric state specificity in coiled coils, J. Am. Chem. Soc. 128 (2006) 15499–15510.

[60] M. Mihajlovic, T. Lazaridis, Antimicrobial peptides in toroidal and cylindrical pores, Biochim. Biophys. Acta Biomembr. 1798 (2010) 1485–1493.

[61] S. Qian, W.C. Wang, L. Yang, H.W. Huang, Structure of the alamethicin pore reconstructed by X-ray diffraction analysis, Biophys. J. 94 (2008) 3512–3522.

[62] M.R.R. de Planque, J.A. Killian, Protein–lipid interactions studied with designed transmembrane peptides: role of hydrophobic matching and interfacial anchoring (Review), Mol. Membr. Biol. 20 (2003) 271–284.

[63] O.S. Andersen, R.E. Koeppe, Bilayer thickness and membrane protein function: an energetic perspective, Annu. Rev. Biophys. Biomol. Struct. 36 (2007) 107–130.

[64] K. He, S.J. Ludtke, H.W. Huang, D.L. Worcester, Antimicrobial peptide pores in membranes detected by neutron in-plane scattering, Biochemistry 34 (1995) 15614–15618.

[65] P. Pieta, J. Mirza, J. Lipkowski, Direct visualization of the alamethicin pore formed in a planar phospholipid matrix, Proc. Natl. Acad. Sci. U. S. A. 109 (2012) 21223–21227.

[66] A.D. Milov, R.I. Samoilova, Y.D. Tsvetkov, M. De Zotti, F. Formaggio, C. Toniolo, J.W. Handgraaf, J. Raap, Structure of self-aggregated alamethicin in ePC membranes detected by pulsed electron–electron double resonance and electron spin echo envelope modulation spectroscopies, Biophys. J. 96 (2009) 3197–3209.

[67] N. Dan, S.A. Safran, Effect of lipid characteristics on the structure of transmembrane proteins, Biophys. J. 75 (1998) 1410–1414.

[68] R.S. Cantor, Size distribution of barrel-stave aggregates of membrane peptides: influence of the bilayer lateral pressure profile, Biophys. J. 82 (2002) 2520–2525.

[69] M.S.P. Sansom, Alamethicin and related peptaibols—model ion channels, Eur. Biophys. J. 22 (1993) 105–124.

[70] K. Asami, T. Okazaki, Y. Nagai, Y. Nagaoka, Modifications of alamethicin ion channels by substitution of Glu-7 for Gln-7, Biophys. J. 83 (2002) 219–228.

[71] R. Chiriac, T. Luchian, pH modulation of transport properties of alamethicin oligomers inserted in zwitterionic-based artificial lipid membranes, Biophys. Chem. 130 (2007) 139–147.

[72] A.J. Krauson, J. He, W.C. Wimley, Gain-of-function analogues of the pore-forming peptide melittin selected by orthogonal high-throughput screening, J. Am. Chem. Soc. 134 (2012) 12732–12741.

[73] G. Boheim, H.A. Kolb, Analysis of multi-pore system of alamethicin in a lipid-membrane. 1. Voltage jump current relaxation measurements, J. Membr. Biol. 38 (1978) 99–150.

[74] V. Rizzo, S. Stankowski, G. Schwarz, Alamethicin incorporation in lipid bilayers — a thermodynamic study, Biochemistry 26 (1987) 2751–2759.

[75] E.S. Salnikov, M.D. Zotti, F. Formaggio, X. Li, C. Toniolo, J.D.J. O'Neil, J. Raap, S.A. Dzuba, B. Bechinger, Alamethicin topology in phospholipid membranes by oriented solid-state NMR and EPR spectroscopies: a comparison, J. Phys. Chem. 113 (2009) 3034–3042.

[76] D. Maisch, P. Wadhwani, S. Afonin, C. Bottcher, B. Koksch, A.S. Ulrich, Chemical labeling strategy with (R)- and (S)-trifluoromethylalainine for solid state F-19 NMR analysis of peptaibols in membranes, J. Am. Chem. Soc. 131 (2009)(15596–+).

[77] D. Marsh, Orientation and peptide–lipid interactions of alamethicin incorporated in phospholipid membranes: polarized infrared and spin-label EPR spectroscopy, Biochemistry 48 (2009) 729–737.

[78] C. Choma, H. Gratkowski, J.D. Lear, W.F. DeGrado, Asn-mediated self-association of a model transmembrane helix, Nat. Struct. Biol. 7 (2000) 161–166.

[79] J.P. Dawson, J.S. Weinger, D.M. Engelman, Motifs of Ser and Thr can drive association of transmembrane helices, J. Mol. Biol. 316 (2002) 799–805.

[80] J.M. Zhang, T. Lazaridis, Calculating the free energy of association of transmembrane helices, Biophys. J. 91 (2006) 1710–1723.

[81] J.M. Zhang, T. Lazaridis, Transmembrane helix association affinity can be modulated by flanking and noninterfacial residues, Biophys. J. 96 (2009) 4418–4427.

[82] M. Criado-Sancho, J. Casas-Vazquez, D. Jou, Non-equilibrium thermodynamic potential and flux fluctuation theorem, Phys. Lett. A 373 (2009) 3301–3303.

[83] R.J. Taylor, R. Delevie, Reversed alamethicin conductance in lipid bilayers, Biophys. J. 59 (1991) 873–879.

[84] W.P. Russ, D.M. Engelman, TOXCAT: a measure of transmembrane helix association in a biological membrane, Proc. Natl. Acad. Sci. U. S. A. 96 (1999) 863–868.

[85] H. Duclohier, Helical kink and channel behaviour: a comparative study with the peptaibols alamethicin, trichotoxin and antiamoebin, Eur. Biophys. J. Biophys. 33 (2004) 169–174.